

Supplementary Information for

**Crystallinity regulation induced organics degradation on
Ultra-thin 2D Co₃O₄/SiO₂ Nanosheets: the critical trigger
of oxygen vacancy**

Wenhui Bai, Hongze Lu, Yang Liu, Xue Yuan, Yuejie Ai, Lidong Wang and Zhe
Chen**

*MOE Key Lab of Resources and Environmental System optimization, College of
Environmental Science and Engineering, North China Electric Power University,
Beijing 102206, P. R. China.*

*Email: chenz@ncepu.edu.cn (Prof. Zhe Chen); wld@ncepu.edu.cn (Prof. Lidong
Wang)*

Text S1. Sources of chemicals.

Text S2. PMS utilization ratio calculation formula.

Text S3. Electrochemical analysis tests.

Text S4. Methods for measuring the concentration of active species.

Text S5. The degradation rate (k) of SMX by different active species.

Text S6. The HPLC methods in the experiment section.

Fig. S1. SEM image of Hemi-Co₃O₄/SiO₂.

Fig. S2. The SMX removal by individual PMS and Hemi-Co₃O₄/SiO₂.

- Fig. S3.** The total organic carbon content in different catalyst/PMS systems.
- Fig. S4.** The SMX degradation activity with Hemi-Co₃O₄/SiO₂ at different pH.
- Fig. S5.** The SMX degradation by Hemi-Co₃O₄/SiO₂ in the atmosphere and nitrogen-bubbling conditions.
- Fig. S6.** The FTIR spectra of bulk cobalt oxide and Hemi-Co₃O₄/SiO₂.
- Fig. S7.** The I-t curves of Hemi-Co₃O₄/SiO₂.
- Fig. S8.** The effect of leaching solution of Hemi-Co₃O₄/SiO₂ on the degradation property of SMX.
- Fig. S9.** The EPR spectra of SO₄•⁻ after the reaction obtained using DMPO as spin-trapping agents.
- Fig. S10.** The N₂ adsorption–desorption isotherms of Hemi-Co₃O₄/SiO₂, A-Co₃O₄/SiO₂ and C-Co₃O₄/SiO₂.
- Fig. S11.** The effect of different real water samples on SMX removal efficiency.
- Fig. S12.** The XRD of Hemi-Co₃O₄/SiO₂ before and after the reaction.
- Fig. S13.** Degradation performance of Hemi-Co₃O₄/SiO₂ on various refractory drugs.
- Fig. S14.** The optimized structures of (a) bulk cobalt oxide, (b) C-Co₃O₄ and (c) Hemi-Co₃O₄.
- Fig. S15.** The optimized structures of (a) isolated PMS, (b) bulk cobalt oxide@PMS

and (c) C-Co₃O₄@PMS in Type II mode.

Fig. S16. The difference charge density of (a) bulk cobalt oxide @PMS and (b) C-Co₃O₄@PMS systems. The iso-surface value was set as 0.003 e/Bohr³, and the yellow and cyan bubbles were represented as the charge accumulation and reduction, respectively.

Fig. S17. The optimized structures of reaction intermediates of ¹O₂ generation on C-Co₃O₄.

Table S1. The adsorption free energies of C-Co₃O₄@PMS and bulk cobalt oxide@PMS in two types mode.

Table S2. Economic Evaluations for SMX removal through different advanced oxidation processes (AOPs).

Table S3. Comparison of catalytic activities between Co₃O₄/SiO₂ catalysts and the previous reports.

Table S4. The degradation of various refractory drugs with Hemi-Co₃O₄/SiO₂.

Table S5. Percentage of peak area of cobalt ions of different valence states in XPS.

Table S6. Percentage of peak areas of different oxygen species in XPS.

Table S7. The concentration of SO₄•⁻ in solution after reaction.

Text S1. Sources of chemicals

All chemicals were of analytically pure reagent and used without further purification. The $\text{CoCl}_2 \cdot 6\text{H}_2\text{O}$, NaOH, tert-butanol (TBA), Methanol, p-benzoquinone (p-BQ), and furfuryl alcohol (FFA) and Sulfamethoxazole (SMX) were purchased from Aladdin Company. Peroxymonosulfate (PMS, $\text{KHSO}_5 \cdot 0.5\text{KHSO}_4 \cdot 0.5\text{K}_2\text{SO}_4$) was purchased from Alfa Aesar. L-hisditine ($\text{C}_6\text{H}_9\text{N}_3\text{O}_2$) was purchased from TCI. The acetone was purchased from Sinopharm Co, Ltd, and the sodium thiosulfate ($\text{Na}_2\text{S}_2\text{O}_3 \cdot 5\text{H}_2\text{O}$) from Macklin Company. All the aqueous solutions were prepared by using Milli-Q water.

Text S2. PMS utilization ratio calculation formula

Eq. S1:
$$\text{PMS utilization ratio} = \frac{\Delta n(\text{pollutant})}{\Delta n(\text{PMS})} \times 100\%$$

In the equation, $\Delta n(\text{SMX})$ represented the molar amount of pollutant removed and $\Delta n(\text{PMS})$ denoted the molar amount of PMS consumed.

Text S3. Electrochemical analysis tests.

The electrochemical analysis was carried out on electrochemical workstation (Koster CS3104). Pt wire and Ag/AgCl electrode were used as the counter and reference electrodes, respectively, while catalyst-modified glassy carbon served as the working electrode. The catalyst ink was prepared by sufficiently sonicating the mixture

of the catalyst (2 mg), isopropyl alcohol (0.74 mL), Nafion solution (0.02 mL), and DI H₂O (0.24 mL). The glass carbon was then modified with the catalyst ink (10 µL) to achieve the desired catalyst loading amount (0.1 mg cm⁻²). PMS and SMX were added at given intervals to final concentrations of 50 mg L⁻¹ and 20 mg L⁻¹. Test results: PMS was added in 21 min and SMX was added in 42 min. There was no obvious current response.

Text S4. Methods for measuring the concentration of active species.

Eq. S2:
$$N_x = \frac{A_x G_x}{A_s G_s} N_s$$

In the equation, (N) represents the spin number of the sample, (A) represents the line integral area of the spectrum, (G) represents the amplification factor of the test, and (s) represents the standard sample while (x) represents the unknown sample.

Text S5. The degradation rate (k) of SMX by different active species.

Eq. S3:
$$k = \frac{(1 - m_x) - (1 - n_x)}{(1 - m_x)} k_x$$

In the equation, (m_x) Percentage of undegraded SMX without scavengers in 2 min, (n_x) Percentage of undegraded SMX with scavengers in 2 min, and (k_x) Rate constants for different catalysts in 2 min.

Text S6. The HPLC methods in the experiment section.

All the samples under text were filtered with 0.22 µm polyethersulfone syringe

membrane filter to determine the concentration via HPLC (Agilent 1260 Infinity II, USA) with an Agilent InfinityLab Poroshell 120 EC-C18 column (4.6×150 mm, $4 \mu\text{m}$).

BPA: The mobile phase was a mixture of 70% methanol and 30% water. The flow rate and injection volumes were 0.5 mL/min and $10 \mu\text{L}$, respectively. The detector wavelength was set at 225 nm. **CBZ:** The mobile phase was a mixture of 40% methanol and 60% water. The flow rate and injection volumes were 0.5 mL/min and $10 \mu\text{L}$, respectively. The detector wavelength was set at 210 nm. **ATZ:** The mobile phase was a mixture of 20% methanol and 80% water. The flow rate and injection volumes were 0.5 mL/min and $10 \mu\text{L}$, respectively. The detector wavelength was set at 220 nm. **SMX:** The mobile phase was a mixture of 25% (0.1% Formic acid) and 75% water. The flow rate and injection volumes were 0.6 mL/min and $20 \mu\text{L}$, respectively. The detector wavelength was set at 554 nm.

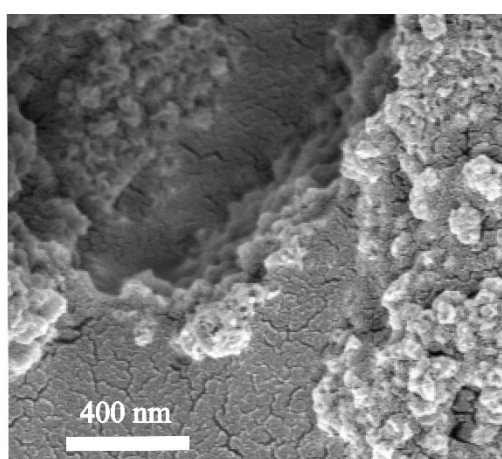


Fig. S1. SEM image of Hemi-Co₃O₄/SiO₂

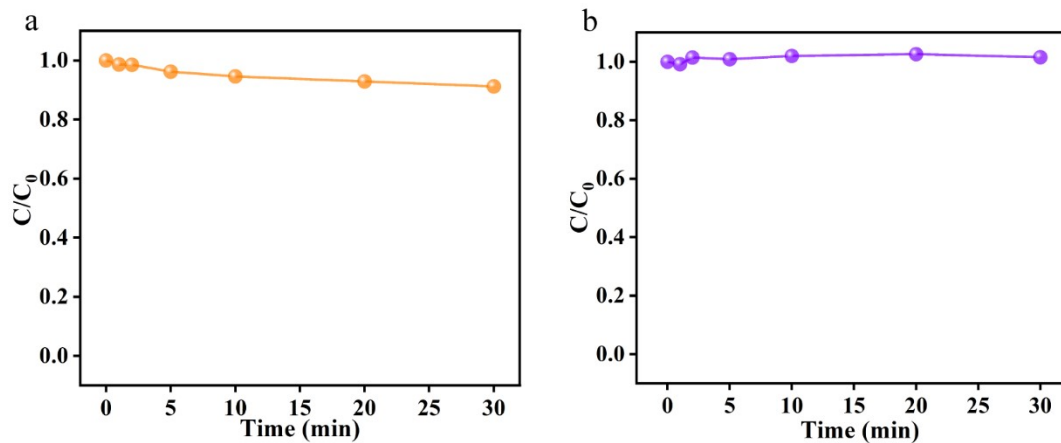


Fig. S2. (a)The SMX removal by individual PMS. $[\text{SMX}] = 20 \text{ mg/L}$, $[\text{PMS}] = 0.12 \text{ g/L}$. (b)The SMX removal by individual Hemi- $\text{Co}_3\text{O}_4/\text{SiO}_2$. $[\text{SMX}] = 20 \text{ mg/L}$, $[\text{Catalyst}] = 0.1 \text{ g/L}$.

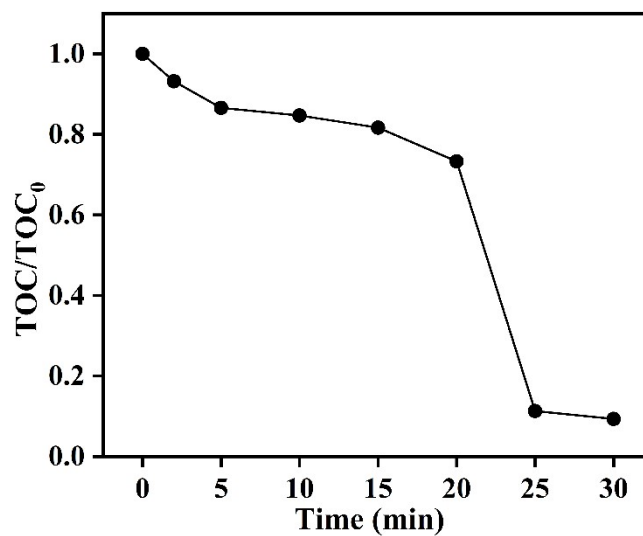


Fig. S3. The total organic carbon content in Hemi- $\text{Co}_3\text{O}_4/\text{SiO}_2/\text{PMS}$ systems. Reaction conditions: $[\text{Hemi-}\text{Co}_3\text{O}_4/\text{SiO}_2] = 0.1 \text{ g/L}$, $[\text{PMS}] = 0.12 \text{ g/L}$, $[\text{SMX}] = 20 \text{ mg/L}$.

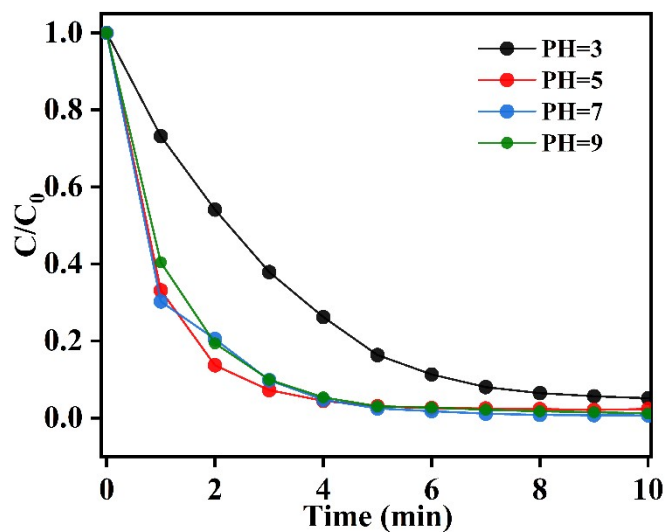


Fig. S4. The SMX degradation activity with Hemi-Co₃O₄/SiO₂ at different pH.

Reaction conditions: [Hemi-Co₃O₄/SiO₂] = 0.1 g/L, [PMS] = 0.12 g/L, [SMX] = 20 mg/L.

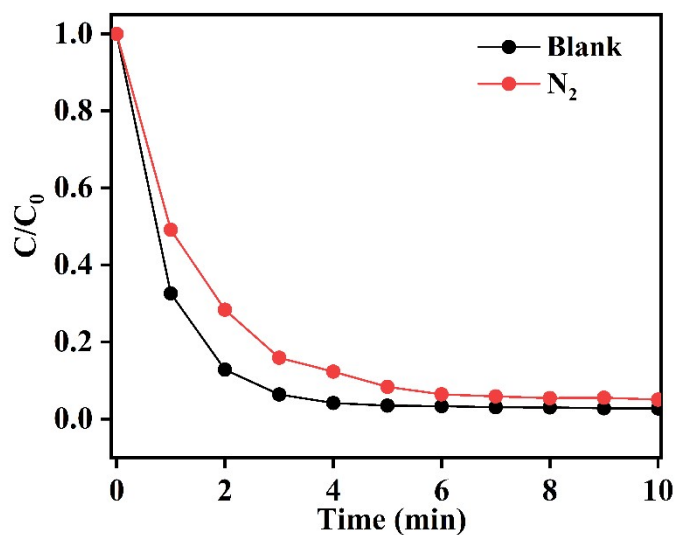


Fig. S5. The SMX degradation by Hemi-Co₃O₄/SiO₂ in the atmosphere and nitrogen-

bubbling conditions. Reaction conditions: [Hemi-Co₃O₄/SiO₂] = 0.1 g/L, [PMS] =

0.12 g/L, [SMX] = 20 mg/L, [initial pH] = 5.3.

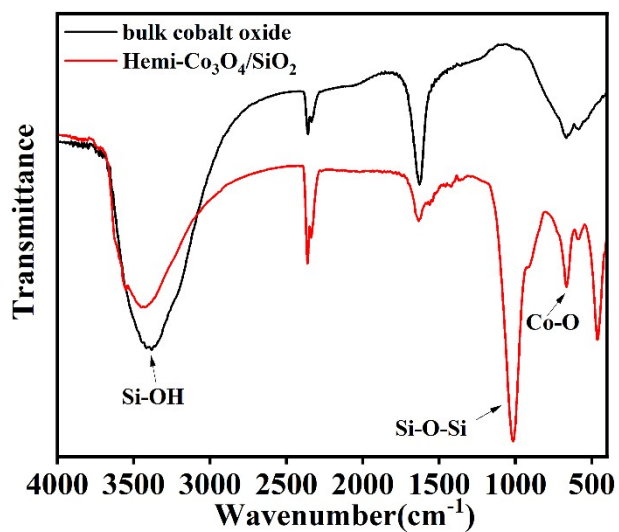


Fig. S6. The FTIR spectra of bulk cobalt oxide and Hemi- $\text{Co}_3\text{O}_4/\text{SiO}_2$.

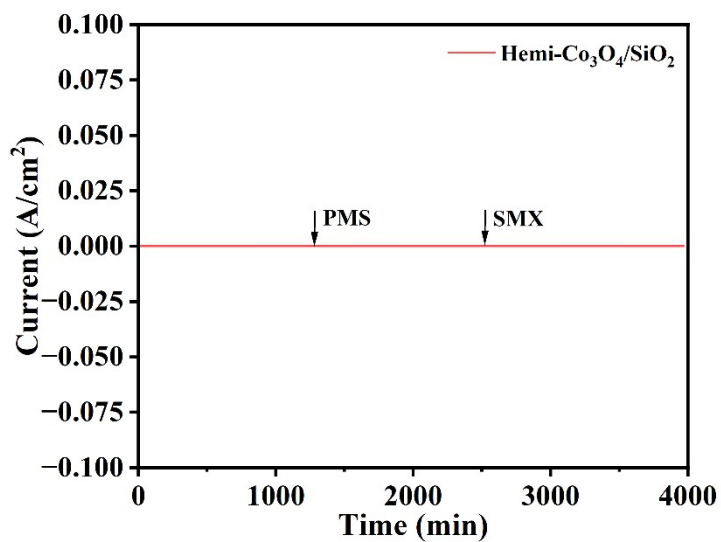


Fig. S7. The I-t curve of Hemi- $\text{Co}_3\text{O}_4/\text{SiO}_2$

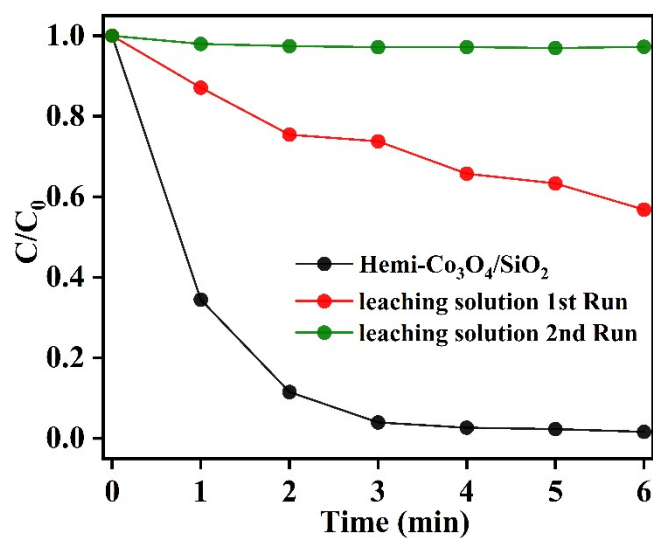


Fig. S8. The activity of leaching cobalt ions from Hemi-Co₃O₄/SiO₂ on the degradation of SMX. Reaction conditions: [PMS] = 0.12 g/L, [SMX] = 20 mg/L.

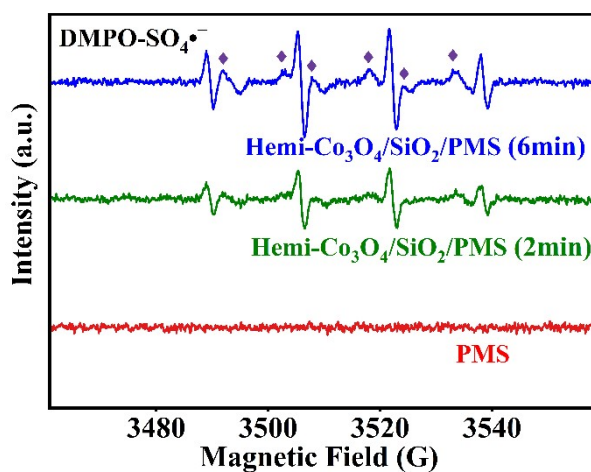


Fig. S9. The EPR spectra of SO₄•⁻ after the reaction obtained using DMPO as spin-trapping agents.

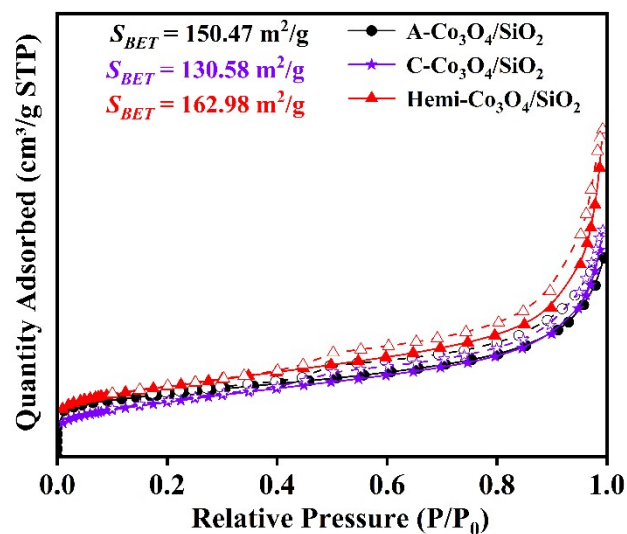


Fig. S10. The N_2 adsorption–desorption isotherms of Hemi- $\text{Co}_3\text{O}_4/\text{SiO}_2$, A- $\text{Co}_3\text{O}_4/\text{SiO}_2$ and C- $\text{Co}_3\text{O}_4/\text{SiO}_2$.

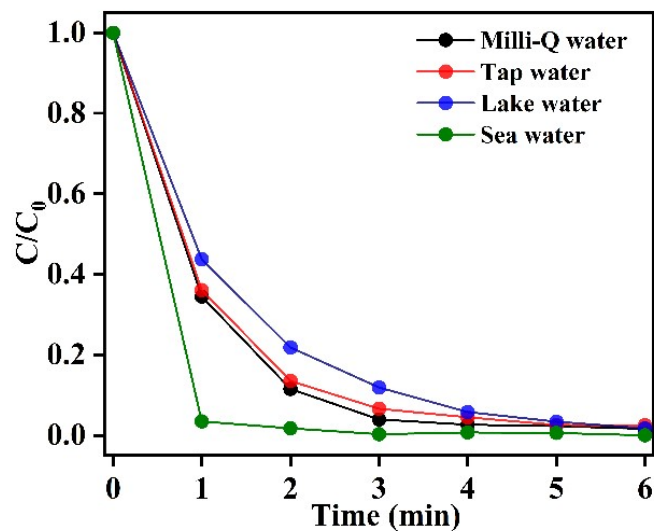


Fig. S11. The effect of different real water samples on SMX removal efficiency.

Reaction conditions: [$\text{Hemi-Co}_3\text{O}_4/\text{SiO}_2$] = 0.1 g/L, [PMS] = 0.12 g/L, [SMX] = 20

mg/L.

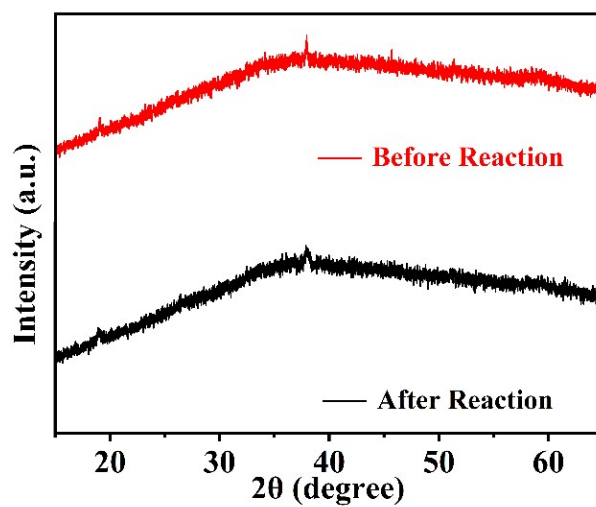


Fig. S12. The XRD of Hemi-Co₃O₄/SiO₂ before and after the reaction.

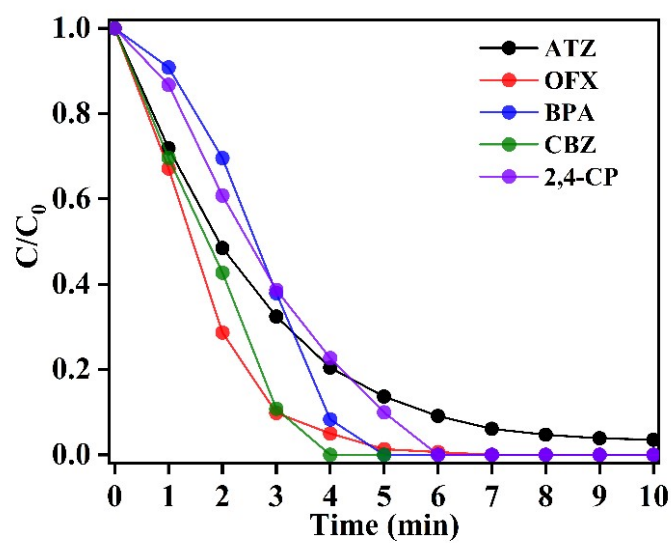


Fig. S13. Degradation performance of Hemi-Co₃O₄/SiO₂ on various refractory drugs.

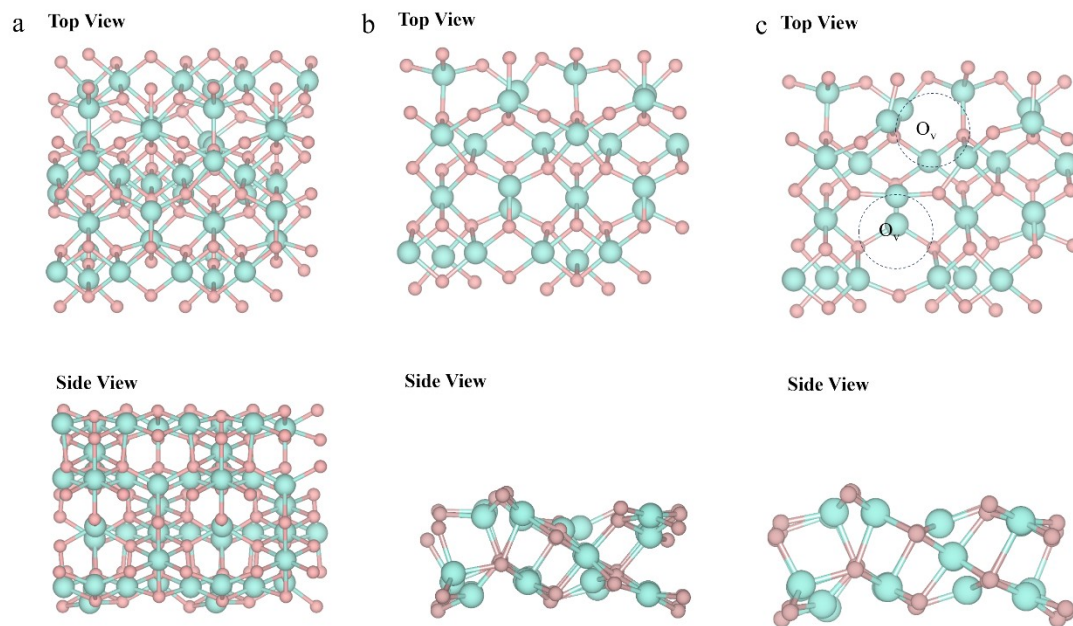


Fig. S14. The optimized structures of (a) bulk cobalt oxide, (b) C-Co₃O₄ and (c) Hemi-Co₃O₄.

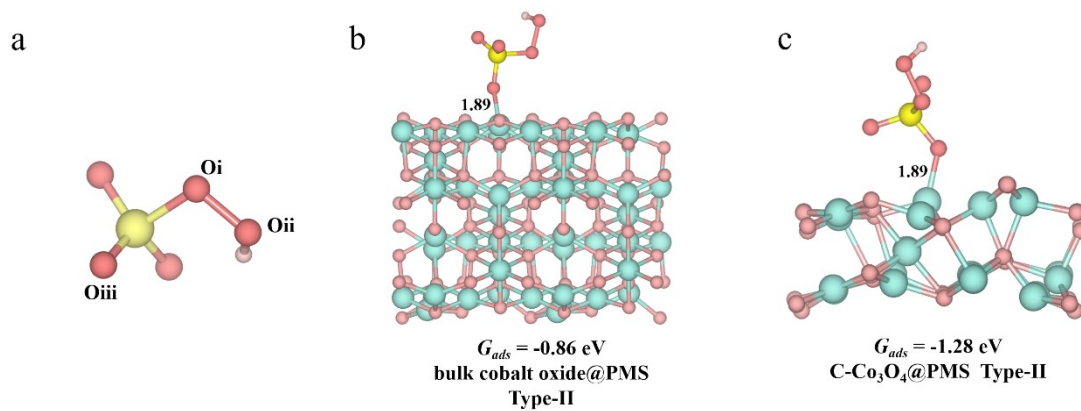


Fig. S15. The optimized structures of (a) isolated PMS, (b) bulk cobalt oxide@PMS and (c) C-Co₃O₄@PMS in Type II mode.

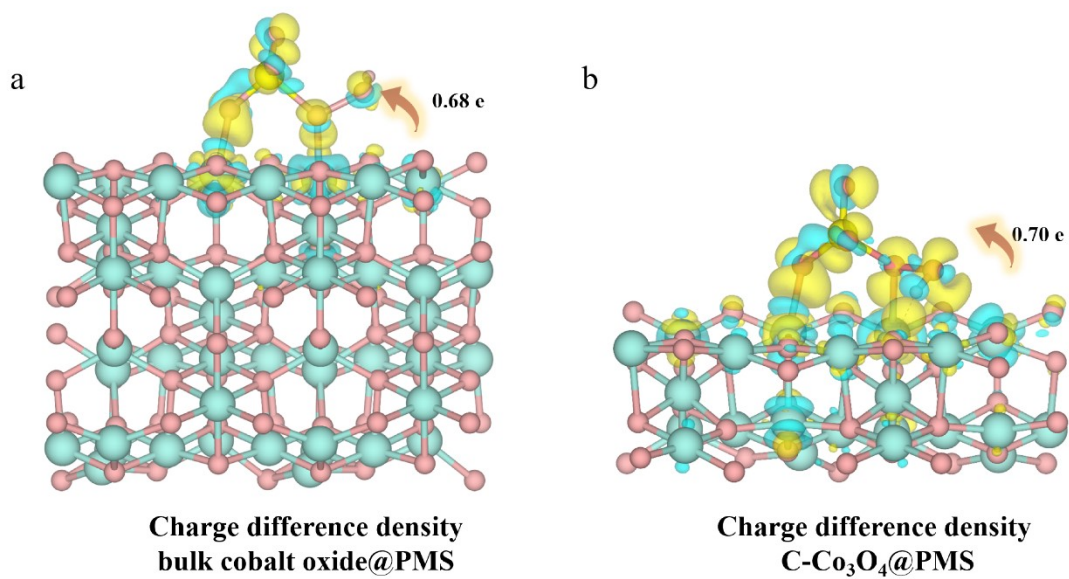


Fig. S16. The difference charge density of (a) bulk cobalt oxide @PMS and (b) C-Co₃O₄@PMS systems. The iso-surface value was set as 0.003 e/Bohr³, and the yellow and cyan bubbles were represented as the charge accumulation and reduction, respectively.

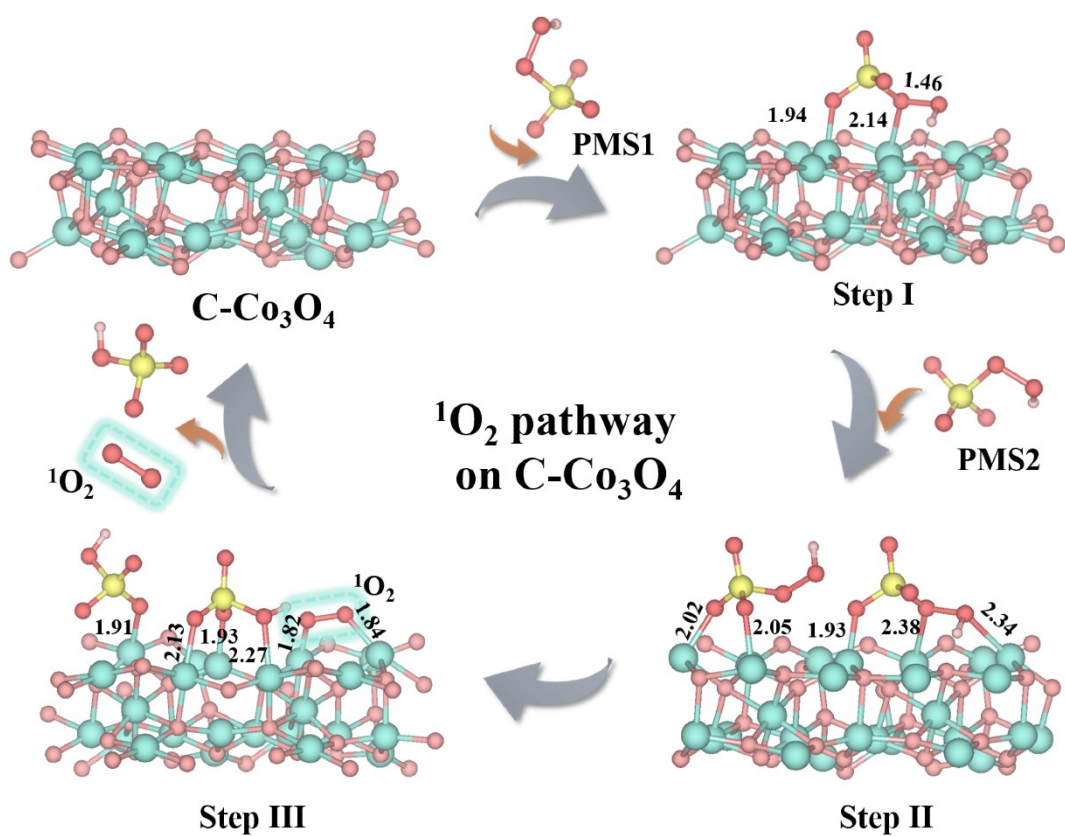


Fig. S17. The optimized structures of reaction intermediates of $^1\text{O}_2$ generation on C- Co_3O_4

Table S1. The adsorption free energies of C- Co_3O_4 @PMS and bulk cobalt oxide@PMS in two types mode.

Co_3O_4 -based catalysts	Binding configurations	$G_{\text{ads}}(\text{eV})$
C- Co_3O_4	Type I	-1.56
	Type II	-1.28
bulk cobalt oxide	Type I	-1.33
	Type II	-0.86

Table S2. Economic Evaluations for SMX removal through different advanced oxidation processes (AOPs).

Catalysts	Reaction system (L)	Time (min)	Contaminant concentration (mg/L)	Oxidant & Chemicals	Energy cost (\$/m ³)	Chemical cost (\$/m ³)	Total cost of treatment (\$/m ³)	Ref.
CoFe/ZSM-5	0.5	60	10	CoFe/ZSM-5 = 0.3 g/L PMS=2 mM	-	1.29	1.29	1
Co/CN-650	0.03	8	10	Co-Cu@g-C ₃ N ₄ -2 = 0.1 g/L PMS=0.5 mM	-	3.26	3.26	2
EB/H ₂ O ₂	-	-	-	EB=25 kGy PMS=10 mM	2.44	0.15-0.30	2.59-2.74	3
CoS _x @SiO ₂	0.05	10	5	CoS _x @SiO ₂ = 0.2 g/L PMS=0.2 mM	-	4.58	4.58	4
Co _x Fe _{1-x} WO ₄	0.1	15	10	Co _x Fe _{1-x} WO ₄ PMS=0.33 mM	-	0.732	0.732	5

Hemi-Co ₃ O ₄ /SiO ₂	0.05	6	20	Hemi-Co ₃ O ₄ /SiO ₂ =0.1g/L PMS=0.39 mM	0.588	0.588	This Work
---	------	---	----	---	-------	-------	--------------

Note: Calculated amounts were approximate.

PMS cost = 1.3 \$/kg; FeSO₄•7H₂O cost = 1.57 \$/kg; CoCl₂•6H₂O cost = 6.71 \$/kg; TAA cost =2.09 \$/kg; FeCl₂•4H₂O cost =1.23 \$/kg;

Na₂WO₄•2H₂O cost = 9.25 \$/kg; Co(NO₃)₂•6H₂O cost = 8.37 \$/kg; TMAH cost = 2.21 \$/kg; TEOS cost =1.54 \$/kg; FeCl₂ cost =1.09 \$/kg;

C₃H₆N₆ = cost = 0.59 \$/kg; Ethylene glycol cost = 0.70 \$/kg; citric acid cost = 0.29 \$/kg; urea=0.63 \$/kg

Table S3 Comparison of catalytic activities between Co₃O₄/SiO₂ catalysts and the previous reports.

Number	Catalyst	Catalyst Dosage (g L ⁻¹)	PMS dosage (mM)	Contaminant (mg L ⁻¹)	pH	Temp. (°C)	k _{obs} (min ⁻¹)	Pathway	Normalized k (min ⁻¹ M ⁻¹)	Ref.
1	Hemi-Co ₃ O ₄ /SiO ₂	0.1	0.39	20	5.8	25	1.10	Radical and nonradical	564.1	This work
2	C-Co ₃ O ₄ /SiO ₂	0.1	0.39	20	5.8	25	0.408	Radical and	209.23	This

								nonradical		work
3	bulk cobalt oxide	0.1	0.39	20	5.8	25	0.225	Radical and nonradical	115.38	This work
4	A-Co ₃ O ₄ /SiO ₂	0.1	0.39	20	5.8	25	0.63	Radical and nonradical	323.08	This work
5	C ₃ N ₅ -Co _{0.59}	0.5	0.8	10	11.03	Room temper ature	0.35158	Radical and nonradical	8.7895	6
6	OMC-Co-T800	0.1	0.65	10	5.8	25	0.1988	Radical	30.58	7
7	Co-N-CNTs	0.1	1	10	6.8	25	0.0008	Radical and nonradical	0.08	8
8	GcN/Co	0.1	1	5	7.1	Room temper ature	0.2028	Radical and nonradical	10.14	9
9	Co-NC-C	0.1	0.33	20	7.08	25	0.038	Radical and nonradical	23.03	10
10	CoNCWS800	0.051	0.6	15	5.14	25	0.1001	Radical and nonradical	49.07	11

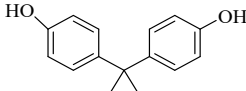
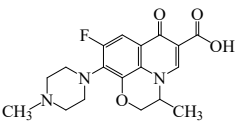
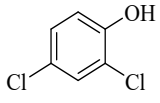
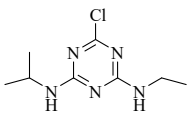
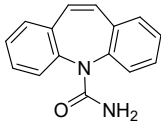
11	CoS _x @SiO ₂	0.2	0.2	5	5.1	25	0.7286	Radical and nonradical	91.075	4
12	CoFeO ₄	0.1	0.2	2.53	6	room temperature	0.1172	Radical	14.8258	12
13	Co-Fe/NC _{0.7} @GCS	0.4	0.5	30	5.76	room temperature	0.101	Radical and nonradical	15.15	13
14	FeCo-BC	0.1	0.4	10	3.4	25	0.749	Radical and nonradical	187.29	14
15	CoMn ₂ O ₄	0.2	0.2	12.6	7	room temperature	0.21		66.15	15
16	Co/CoO/Co ₉ S ₈ @NSOC	0.1	0.8	20	7.88	25	1.3	Radical and nonradical	325	16
17	LCo	0.15	0.4	2.5	11.88	30	0.2133	Radical	11.85	17
18	Fe-Co-O-g-C ₃ N ₄	0.2	0.8	10	3.4	25	0.085	Radical and nonradical	53.125	18
19	Co ₃ O ₄ @NCNTs	0.1	0.65	20	6.67	25	0.2224	Radical and nonradical	68.43	19

								nonradical		
20	Co _{0.70} Fe _{0.30} WO ₄	0.1	0.325	10	7	25	0.272	Radical	83.69	5
21	CoOOH/BC	0.3	0.65	40	5.2	room temperature	0.443	Radical and nonradical	90.87	20
22	B-CoOOH	0.1	0.3	10	9	room temperature	1.65	Radical and nonradical	550	21
23	A-Co-CN/g-C ₃ N ₄	0.2	1.3	20	6	room temperature	0.2601	Radical and nonradical	20.07	22

Note: The normalized kinetics were obtained via normalizing reaction rate constant (k_{obs}) to the dosage of catalyst, oxidants, and organics via

Eq. S4:
$$Normalized\ k = \frac{k_{obs} \cdot c_{SMX}}{c_{Catalyst} \cdot c_{PS}}$$

Table S4. The Degradation of various refractory drugs with Hemi-Co₃O₄/SiO₂.

Enter	Contaminants	Structural formula	Time (min)	Conversion (%)	k (mn ⁻¹)
1	Bisphenol A		2	30.4%	0.182
2	Ofloxacin		2	71.3%	0.625
3	2,4-dichlorophenol		2	39.2%	0.249
4	Atrazine		2	51.5%	0.362
5	Carbamazepine		2	57.3%	0.425

Note: k value is the rate constant for degradation of different pollutants over two min.

Ct: the pollutant concentration at two min (t), C₀ is the initial pollutant concentration

$$\text{Eq. S5: } k = \frac{-\ln\left(\frac{C_t}{C_0}\right)}{t}$$

Table S5. Percentage of peak area of cobalt ions of different valence states in XPS.

Catalyst	Percentage of Co ²⁺ peak	Percentage of Co ³⁺ peak
	area (%)	area (%)
Hemi-Co ₃ O ₄ /SiO ₂	52.2	47.8
A-Co ₃ O ₄ /SiO ₂	45.4	55.6
C-Co ₃ O ₄ /SiO ₂	41.1	58.9

Note: m: Percentage of Co²⁺ peak area (%); n: Percentage of Co³⁺ peak area (%)

$$\text{Eq. S6: } \frac{\text{Co}^{2+} / \text{Co}^{3+}}{m/n}$$

Table S6. Percentage of peak areas of different oxygen species in XPS.

Catalyst	Percentage of O _{Latt}	Percentage of O _{ada}	Percentage of O _{surf}
	peak area (%)	peak area (%)	peak area (%)
Hemi-Co ₃ O ₄ /SiO ₂	44.0	41.6	14.1
A-Co ₃ O ₄ /SiO ₂	53.4	34.9	11.7
C-Co ₃ O ₄ /SiO ₂	62.0	24.5	13.5

Table S7. The concentration of SO₄•⁻ in the solution after the reaction.

Time (min)	Concentration of SO ₄ • ⁻
2	1.789×10 ⁻⁵ mol/L
6	3.702×10 ⁻⁵ mol/L

References

1. Y. Li, X. Zheng, Q. Guo, X. Wang, L. Zhang, W. Zhu and Y. Luo, Activation of peroxymonosulfate by the CoFe/ZSM-5 for efficient sulfamethoxazole degradation, *J. Environ. Chem. Eng.*, 2022, **10**, 107012.
2. H. Zhang, G. Xu and Y. Yu, Co single-atom C₂N₃ activates peroxymonosulfate for efficient degradation of sulfamethoxazole at 4°C: A combined experimental and density functional theory study, *Chem. Eng. J.*, 2023, **476**, 146721.
3. L. Chu, J. Wang, C. Chen, S. He, L. Wojnárovits and E. Takács, Advanced treatment of antibiotic wastewater by ionizing radiation combined with peroxymonosulfate/H₂O₂ oxidation, *J. Cleaner Prod.*, 2021, **321**, 128921.
4. F. Wang, H. Fu, F.-X. Wang, X.-W. Zhang, P. Wang, C. Zhao and C.-C. Wang, Enhanced catalytic sulfamethoxazole degradation via peroxymonosulfate activation over amorphous CoS_x@SiO₂ nanocages derived from ZIF-67, *J. Hazard. Mater.*, 2022, **423**, 126998.
5. F. Zhang, H.-N. Yan, Y.-F. Jin, L.-F. Zhai and M. Sun, Co-Fe synergy in Co_xFe_{1-x}WO₄: The new type peroxymonosulfate activator for sulfamethoxazole degradation, *Chem. Eng. J.*, 2023, **461**, 141989.
6. P. He, C. Gu, B. Tang, Y. Zhou, M. Gan and J. Zhu, Expedient degradation of SMX by high-valent cobalt-oxo species derived from cobalt-doped C₃N₅-activated peroxymonosulfate with the assistance of visible light, *Sep. Purif. Technol.*, 2022, **301**, 122009.

7. H. Zhang, R. Lee Smith, H. Guo and X. Qi, Cobalt cross-linked ordered mesoporous carbon as peroxymonosulfate activator for sulfamethoxazole degradation, *Chem. Eng. J.*, 2023, **472**, 145060.
8. J. Miao, Y. Zhu, J. Lang, J. Zhang, S. Cheng, B. Zhou, L. Zhang, P. J. J. Alvarez and M. Long, Spin-State-Dependent Peroxymonosulfate Activation of Single-Atom M–N Moieties via a Radical-Free Pathway, *ACS Catal.*, 2021, **11**, 9569-9577.
9. D. T. Oyekunle, D. Li, L. Zheng, F. Luo, S. Wang and Z. Chen, Enhanced degradation of organic compounds through the interfacial transfer of electrons in the presence of phosphate and Nitrogen-cobalt doped graphitic carbon, *J. Colloid Interface Sci.*, 2022, **607**, 1641-1650.
10. H. Liu, Z. He, S. Wang and S. Zhao, CoZn-ZIF and melamine co-derived double carbon layer matrix supported highly dispersed and exposed Co nanoparticles for efficient degradation of sulfamethoxazole, *Chem. Eng. J.*, 2023, **469**, 144054.
11. Y. Yu, N. Li, X. Lu, B. Yan, G. Chen, Y. Wang, X. Duan, Z. Cheng and S. Wang, Co/N co-doped carbonized wood sponge with 3D porous framework for efficient peroxymonosulfate activation: Performance and internal mechanism, *J. Hazard. Mater.*, 2022, **421**, 126735.
12. X. Li, Z. Zhao, H. Li and J. Qian, Degradation of organic contaminants in the CoFe₂O₄/peroxymonosulfate process: The overlooked role of Co(II)-PMS complex, *Chem. Eng. J. Adv.*, 2021, **8**, 100143.
13. A. Wang, J. Ni, W. Wang, D. Liu, Q. Zhu, B. Xue, C.-C. Chang, J. Ma and Y. Zhao, MOF Derived Co–Fe nitrogen doped graphite carbon@crosslinked magnetic chitosan Micro–nanoreactor for environmental applications: Synergy enhancement effect of adsorption–PMS activation, *Appl. Catal., B*, 2022, **319**, 121926.
14. S. Wang and J. Wang, Bimetallic and nitrogen co-doped biochar for peroxymonosulfate (PMS) activation to degrade emerging contaminants, *Sep. Purif. Technol.*, 2023, **307**, 122807.
15. T.-B. Nguyen, C. P. Huang, R.-a. Doong, M.-H. Wang, C.-W. Chen and C.-D. Dong, Manipulating the morphology of 3D flower-like CoMn₂O₄ bimetallic catalyst for enhancing the activation of peroxymonosulfate toward the degradation of selected persistent pharmaceuticals in water, *Chem. Eng. J.*, 2022, **436**, 135244.
16. Y. Jiang, J. Wang, B. Liu, W. Jiang, T. Zhou, Y. Ma, G. Che and C. Liu, Superhydrophilic N,S,O-doped Co/CoO/Co₉S₈@carbon derived from metal-

- organic framework for activating peroxymonosulfate to degrade sulfamethoxazole: Performance, mechanism insight and large-scale application, *Chem. Eng. J.*, 2022, **446**, 137361.
17. Y. Chen, H. Zhang, Z. Xiong, Y. Wang, S. Peng, J. Wang and Y. Guo, Lithium cobalt oxide with excellent electron mobility: An efficient activator of peroxymonosulfate for the degradation of sulfamethoxazole, *Chem. Eng. J.*, 2022, **445**, 136702.
 18. S. Wang, Y. Liu and J. Wang, Peroxymonosulfate Activation by Fe–Co–O-Codoped Graphite Carbon Nitride for Degradation of Sulfamethoxazole, *Environ. Sci. Technol.*, 2020, **54**, 10361-10369.
 19. J. Ye, J. Dai, C. Li and Y. Yan, Lawn-like Co₃O₄@N-doped carbon-based catalytic self-cleaning membrane with peroxymonosulfate activation: A highly efficient singlet oxygen dominated process for sulfamethoxazole degradation, *Chem. Eng. J.*, 2021, **421**, 127805.
 20. M. Xiong, B. Chai, G. Fan, X. Zhang, C. Wang and G. Song, Immobilization CoOOH nanosheets on biochar for peroxymonosulfate activation: Built-in electric field mediated radical and non-radical pathways, *J. Colloid Interface Sci.*, 2023, **638**, 412-426.
 21. H. Zeng, H. Zhu, J. Deng, Z. Shi, H. Zhang, X. Li and L. Deng, New insight into peroxymonosulfate activation by CoAl-LDH derived CoOOH: Oxygen vacancies rather than Co species redox pairs induced process, *Chem. Eng. J.*, 2022, **442**, 136251.
 22. M. Qian, X.-L. Wu, M. Lu, L. Huang, W. Li, H. Lin, J. Chen, S. Wang and X. Duan, Modulation of Charge Trapping by Island-like Single-Atom Cobalt Catalyst for Enhanced Photo-Fenton-Like reaction, *Adv. Funct. Mater.*, 2023, **33**, 2208688.